Available online at www.sciencedirect.com
SCIENCE DIRECT®
Journal of Computational Physics 203 (2005) 112–128
JOURNAL OF COMPUTATIONAL PHYSICS
www.elsevier.com/locate/jcp

Numerical analysis on magnetic levitation of liquid metals, using a spectral finite difference scheme

Kichang Im *, Yoshihiro Mochimaru

Department of International Development Engineering, Tokyo Institute of Technology, Ookayama, Meguro-ku, Tokyo 152-8550, Japan

Received 7 April 2004; received in revised form 28 July 2004; accepted 10 August 2004
Available online 18 October 2004

Abstract

A spectral finite difference method is applied to analysis on magnetic levitation as a major unsteady-state problem in magnetohydrodynamics. Vorticity-stream function formulation is introduced in conjunction with Maxwell's equations, and the non-linear term of Ohm's law for a liquid metal is included. For the purpose of analysis treated is a liquid metal occupying a volume such that no shear stresses and no normal velocity components on the free surface are used as dynamic boundary conditions. Externally applied electromagnetic fields consist of no electromagnetic field at infinity and fields produced by circular coils placed horizontally near the liquid metal. Presented are lift force, magnetic fields and flow fields for several parameters. Numerical data for high viscosity on dimensionless force with the dimensionless vertical coil position are qualitatively in good agreement with experimental data for a solid metal [J. Appl. Phys. 23 (1952) 545]. The effects of the Reynolds number, the Strouhal number and the number of the external coil(s) on levitation force, the magnetic field and the flow field are clarified.

Keywords: Spectral method; Finite difference; Magnetic levitation; Levitation force

1. Introduction

Magnetic levitation for metallic substances has been used to melt, stir, heat and evaporate electrically conducting liquids at a high temperature, and to measure thermophysical properties such as density, surface

* Corresponding author. Tel.: +81 3 5734 2767; fax: +81 3 5734 3688.
E-mail address: imkc@ide.titech.ac.jp (K. Im).

0021-9991/$ - see front matter © 2004 Elsevier Inc. All rights reserved.
doi:10.1016/j.jcp.2004.08.008

tension, viscosity, electrical conductivity, and thermal properties of clean liquid metals [1,2]. Many theoretical and experimental studies have been done to provide the metallurgist with electromagnetic knowledge applied to magnetic levitation [3–9]. To avoid difficulty in solving Maxwell's equations, most theoretical and numerical studies for levitation melting have neglected the non-linear term in Ohm's law for a liquid metal [4,8,9].

On the other hand, spectral schemes have been used recently along with a finite difference scheme and a finite element one for a numerical analysis of hydrodynamic and magnetohydrodynamic phenomena. Although a spectral finite difference (SFD) scheme is a kind of spectral methods in principle, it is different in nature from conventional spectral finite element methods [10], while SFD schemes in heat and fluid flow have been developed and their effectiveness has been found [10], a few of those in magnetohydrodynamics has been developed only to get a steady-state solution [11,12]. In this paper, magnetic levitation of liquid metals, which is one of unsteady-state problems, is analyzed numerically with Ohm's law included the non-linear term, using a SFD scheme.

The paper is organized as follows: Section 2 describes analysis using a SFD scheme. In Section 3, numerical results for levitation melting under the isothermal condition are presented. Conclusions are given in Section 4.

2. Analysis

2.1. Basic equations

The equation of motion and the equation of continuity only for a liquid metal field are expressed as

$$\rho\left\{\frac{\partial}{\partial t}\boldsymbol{v}+(\boldsymbol{v}\cdot\nabla)\boldsymbol{v}\right\}=\nabla\cdot\boldsymbol{\tau}+\rho\boldsymbol{g}, \tag{1}$$

$$\nabla\cdot\boldsymbol{v}=0, \tag{2}$$

respectively, where ρ is the density, $\boldsymbol{v}$ the velocity vector, τ the stress tensor, and $\boldsymbol{g}$ is the acceleration vector of gravity. The following model of a stress tensor is adopted:

$$\tau_{ij}=\mu d_{ij}-g_{ij}P+H_iB_j-\frac{1}{2}g_{ij}H^kB_k, \tag{3}$$

where μ is the viscosity; d_{ij} the rate of deformation tensor; P the pressure; H_i the magnetic field vector; B_i the magnetic flux density vector; and g_{ij} is the metric tensor.

Maxwell's equations governing the electromagnetic field are expressed as

$$\nabla\times\boldsymbol{E}=-\frac{\partial\boldsymbol{B}}{\partial t}, \tag{4}$$

$$\nabla\times\boldsymbol{H}=\boldsymbol{j}+\frac{\partial\boldsymbol{D}}{\partial t}, \tag{5}$$

$$\nabla\cdot\boldsymbol{B}=0, \tag{6}$$

respectively, where $\boldsymbol{E}$ is the electric field; $\boldsymbol{j}$ the current density; and $\boldsymbol{D}$ is the electric flux density. In the case of a liquid metal, neglecting the displacement current term $\partial\boldsymbol{D}/\partial t$ is a usual assumption. Furthermore, it is assumed that

$$\boldsymbol{B}=\mu_m\boldsymbol{H}, \tag{7}$$

where μ_m is the magnetic permeability. In addition to the above, Ohm's law for a moving medium is used:

$$\boldsymbol{j} = \sigma(\boldsymbol{E} + \boldsymbol{v} \times \boldsymbol{B}), \tag{8}$$

where σ is electrical conductivity.

2.2. Dimensionless governing equations of a liquid metal

Axisymmetric distribution of an alternating current in an external circular coil surrounding a spherical shape of a liquid metal is assumed.

Let (z,r,θ) be a cylindrical coordinate system such that origin is located at the center of the liquid metal and that the z-axis is perpendicular to the coil, and (z,r,θ) is mapped on (R,β,θ) using $z + \mathrm{i}r = \exp(\alpha + \mathrm{i}\beta) = R\exp(\mathrm{i}\beta)$. Then vorticity-stream function formulation of an axisymmetric field is given by

$$\begin{aligned}
&\frac{J}{R^2}\frac{\partial\zeta}{\partial t} + \frac{1}{R}\frac{\partial(\zeta,\psi)}{\partial(R,\beta)} + \frac{1}{R}\frac{\partial}{\partial R}\left(\frac{1}{r}\frac{\partial r}{\partial\beta}\zeta\psi\right) - \frac{1}{R}\frac{\partial}{\partial\beta}\left(\frac{1}{r}\frac{\partial r}{\partial R}\zeta\psi\right)\\
&\quad = \frac{1}{Re}\left\{\left(\frac{\partial^2}{\partial R^2} + \frac{1}{R}\frac{\partial}{\partial R} + \frac{1}{R^2}\frac{\partial^2}{\partial\beta^2}\right)\zeta + \frac{1}{R}\frac{\partial}{\partial R}\left(\frac{R}{r}\frac{\partial r}{\partial R}\zeta\right) + \frac{1}{R^2}\frac{\partial}{\partial\beta}\left(\frac{1}{r}\frac{\partial r}{\partial\beta}\zeta\right)\right\}\\
&\qquad + \frac{1}{R}\frac{\partial(\zeta_B,\psi_B)}{\partial(R,\beta)} + \frac{1}{R}\frac{\partial}{\partial R}\left(\frac{1}{r}\frac{\partial r}{\partial\beta}\zeta_B\psi_B\right) - \frac{1}{R}\frac{\partial}{\partial\beta}\left(\frac{1}{r}\frac{\partial r}{\partial R}\zeta_B\psi_B\right),
\end{aligned} \tag{9}$$

$$-\frac{J}{R^2}\zeta = \left(\frac{\partial^2}{\partial R^2} + \frac{1}{R}\frac{\partial}{\partial R} + \frac{1}{R^2}\frac{\partial^2}{\partial\beta^2}\right)\psi + \frac{1}{R}\frac{\partial}{\partial R}\left(\frac{R}{r}\frac{\partial r}{\partial R}\psi\right) + \frac{1}{R^2}\frac{\partial}{\partial\beta}\left(\frac{1}{r}\frac{\partial r}{\partial\beta}\psi\right), \tag{10}$$

where a is radius of a liquid metal; B_0 the reference magnetic flux density; $U \equiv B_0/\sqrt{\mu_m\rho}$; t the dimensionless time based on a/U; ζ the dimensionless vorticity based on U/a; $r\psi$ the dimensionless stream function based on a^2U; ζ_B the dimensionless magnetic vorticity based on B_0/a; $r\psi_B$ the dimensionless magnetic stream function based on $a\,{}^2B_0$, $Re \equiv (aB_0/\mu)\sqrt{\rho/\mu_m}$, $J \equiv \partial(z,r)/\partial(\alpha,\beta)$.

By integrating the axisymmetric induction equation deduced from Maxwell's equations, we obtain

$$\begin{aligned}
&\frac{J}{R^2}\frac{\partial\psi_B}{\partial t} + \frac{1}{R}\frac{\partial(\psi_B,\psi)}{\partial(R,\beta)} + \frac{1}{R}\psi\frac{1}{r}\frac{\partial(\psi_B,r)}{\partial(R,\beta)} - \frac{1}{R}\psi_B\frac{1}{r}\frac{\partial(\psi,r)}{\partial(R,\beta)}\\
&\quad = \frac{1}{Re\cdot P_m}\left\{\left(\frac{\partial^2}{\partial R^2} + \frac{1}{R}\frac{\partial}{\partial R} + \frac{1}{R^2}\frac{\partial^2}{\partial\beta^2}\right)\psi_B + \frac{1}{R}\frac{\partial}{\partial R}\left(\frac{R}{r}\frac{\partial r}{\partial R}\psi_B\right) + \frac{1}{R^2}\frac{\partial}{\partial\beta}\left(\frac{1}{r}\frac{\partial r}{\partial\beta}\psi_B\right)\right\} + \frac{J}{R^2}\frac{f(t)}{r},
\end{aligned} \tag{11}$$

where $P_m \equiv \mu\sigma\mu_m/\rho$, $f(t)/r$ the constant of integration to be determined ($f(t)$: function only of t). The point $R = 0$ is by no means a singular point in a physical point of view, so that as a necessary condition $f(t) \equiv 0$ is obtained. The relation between the magnetic vorticity and the magnetic stream function is given by

$$-\frac{J}{R^2}\zeta_B = \left(\frac{\partial^2}{\partial R^2} + \frac{1}{R}\frac{\partial}{\partial R} + \frac{1}{R^2}\frac{\partial^2}{\partial\beta^2}\right)\psi_B + \frac{1}{R}\frac{\partial}{\partial R}\left(\frac{R}{r}\frac{\partial r}{\partial R}\psi_B\right) + \frac{1}{R^2}\frac{\partial}{\partial\beta}\left(\frac{1}{r}\frac{\partial r}{\partial\beta}\psi_B\right). \tag{12}$$

Dimensionless velocity components in the z- and r-direction; v_z and v_r are, respectively, given by

$$v_z \equiv \frac{1}{r}\frac{\partial(r\psi)}{\partial r}, \quad v_r \equiv -\frac{\partial\psi}{\partial z}. \tag{13}$$

Dimensionless magnetic flux density components in the z- and r-direction; B_z and B_r are, respectively, given by

$$B_z \equiv \frac{1}{r}\frac{\partial(r\psi_B)}{\partial r}, \quad B_r \equiv -\frac{\partial \psi_B}{\partial z}. \tag{14}$$

2.3. Approximation to Maxwell's equations on an external region of a liquid metal

Electrical conductivity of a vacuum and air is nearly a zero ($\sigma \simeq 0$) so that current density on an external region of a liquid metal is nearly a zero. Then Eq. (5) of an axisymmetric field is approximated to

$$\left(\frac{\partial^2}{\partial R^2}+\frac{1}{R}\frac{\partial}{\partial R}+\frac{1}{R^2}\frac{\partial^2}{\partial \beta^2}\right)\psi_B+\frac{1}{R}\frac{\partial}{\partial R}\left(\frac{R}{r}\frac{\partial r}{\partial R}\psi_B\right)+\frac{1}{R^2}\frac{\partial}{\partial \beta}\left(\frac{1}{r}\frac{\partial r}{\partial \beta}\psi_B\right)=0 \tag{15}$$

if $1 < R < R_n$ or $R_n + h_n < R$.

In the region ($R_n \leqslant R \leqslant R_n + h_n$), Eq. (15) is replaced by

$$\left(\frac{\partial^2}{\partial R^2}+\frac{1}{R}\frac{\partial}{\partial R}+\frac{1}{R^2}\frac{\partial^2}{\partial \beta^2}\right)\psi_B+\frac{1}{R}\frac{\partial}{\partial R}\left(\frac{R}{r}\frac{\partial r}{\partial R}\psi_B\right)+\frac{1}{R^2}\frac{\partial}{\partial \beta}\left(\frac{1}{r}\frac{\partial r}{\partial \beta}\psi_B\right)=-\zeta_B^{\mathrm{e}}, \tag{16}$$

where the dimensionless external magnetic vorticity ζ_B^{e} is produced by a single-loop coil at $R_n \leqslant R \leqslant R_n + h_n$ and $\beta_n \leqslant |\beta| \leqslant \beta_n + \beta_n'$, and given by

$$\zeta_B^{\mathrm{e}} = I_{kn}\cos(St\cdot t)\left\{H(\beta-\beta_n)-H(\beta-\beta_n-\beta_n')+H(\beta+\beta_n)-H(\beta+\beta_n+\beta_n')\right\} \quad (R_n \leqslant R \leqslant R_n+h_n), \tag{17}$$

where $I_{kn} \equiv (a\mu_m I_n)/(A_{\mathrm{coil}}B_0)$; I_n is the peak current in a coil; A_{coil} the cross-section of a coil; $St \equiv a\omega\sqrt{\mu_m\rho}/B_0$, $\omega/2\pi$ the frequency, and $H(\,)$ is the Heaviside step function. Fig. 1 shows a single-loop configuration of the magnetic levitation melting, where $c_{rn} \equiv (R_n + h_n/2)\cos(\beta_n + \beta_n'/2)$, $c_{zn} \equiv (R_n + h_n/2)\sin(\beta_n + \beta_n'/2)$. In case of multi-loop coils, the external magnetic vorticity ζ_B^{e} is superimposed from each contribution of coils.

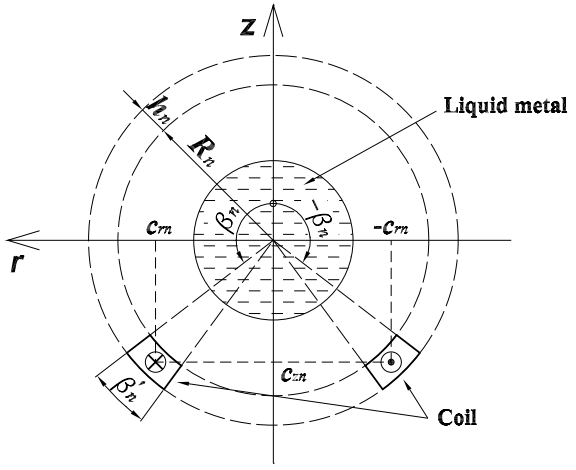

Fig. 1. Example of magnetic levitation melting.

2.4. Spectral formulation

The following form of a solution is considered:

$$\begin{bmatrix} \psi \\ \zeta \end{bmatrix} = \sum_{n=1}^{\infty} \begin{bmatrix} \psi_n(R,t) \\ \zeta_n(R,t) \end{bmatrix} \sin n\beta, \quad \begin{bmatrix} \psi_B \\ \zeta_B \end{bmatrix} = \sum_{n=1}^{\infty} \begin{bmatrix} \psi_{Bn}(R,t) \\ \zeta_{Bn}(R,t) \end{bmatrix} \sin n\beta. \tag{18}$$

2.5. Boundary conditions

As time development of electromagnetic equipment, possible loads of a liquid metal which can be levitated have been considerably increased [6]. For the purpose of analysis treated is a liquid metal occupying a volume such that no shear stresses and no normal velocity components on the free surface are considered as the velocity boundary condition. That is,

$$\psi(R=1,\beta,t) = 0, \tag{19}$$

$$\left(\frac{J}{R^2}\zeta + \frac{1}{J}\frac{\partial J}{\partial R}\frac{\partial \psi}{\partial R} + Re\frac{J}{R^2}B_\alpha B_\beta\right)_{R=1} = 0, \tag{20}$$

where B_α is the dimensionless magnetic flux density component in the α-direction based on B_0, and B_β is the dimensionless magnetic flux density component in the β-direction based on B_0. Eq. (19) leads to

$$\psi_n(1,t) = 0 \quad (n \geqslant 1). \tag{21}$$

Eq. (20) is approximated as

$$\zeta_n(R_{-1},t) - 2\frac{h_{-1}+h_{-2}}{h_{-1}h_{-2}}\psi_n(R_{-1},t) + 2\frac{h_{-1}}{h_{-2}(h_{-1}+h_{-2})}\psi_n(R_{-2},t) + \frac{2}{\pi}Re\int_0^\pi \sin n\beta (B_\alpha B_\beta)_{R=1}\,\mathrm{d}\beta = 0, \tag{22}$$

where $R_0 = 1$, R_{-1} and R_{-2} are R-values at the first and second grid point from $R = 1$ inward, respectively, $h_{-1} = 1 - R_{-1}$, and $h_{-2} = R_{-1} - R_{-2}$.

Magnetic field boundary conditions are

$$\left(\psi_B^{\mathrm{i}} - \psi_B^{\mathrm{e}}\right)_{R=1} = 0, \tag{23}$$

$$\left(\frac{\partial \psi_B^{\mathrm{i}}}{\partial R} - \frac{\partial \psi_B^{\mathrm{e}}}{\partial R}\right)_{R=1} = 0, \tag{24}$$

$$\psi_B(R_\infty,\beta,t) = 0, \tag{25}$$

where R_∞ is the R-value at the virtual boundary equivalent to infinity ($R_\infty \simeq 100$), and superscripts of i and e indicate the internal and external field of a liquid metal, respectively. Eq. (23) leads to

$$\psi_{Bn}^{\mathrm{i}}(1,t) - \psi_{Bn}^{\mathrm{e}}(1,t) = 0 \quad (n \geqslant 1). \tag{26}$$

Eq. (24) is approximated as

$$\frac{2h_0+h_1}{h_0(h_0+h_1)}\psi^{e}_{Bn}(1,t)-\frac{h_0+h_1}{h_0h_1}\psi^{e}_{Bn}(R_1,t)+\frac{h_0}{h_1(h_0+h_1)}\psi^{e}_{Bn}(R_2,t)+\frac{2h_{-1}+h_{-2}}{h_{-1}(h_{-1}+h_{-2})}\psi^{i}_{Bn}(1,t)$$
$$-\frac{h_{-1}+h_{-2}}{h_{-1}h_{-2}}\psi^{i}_{Bn}(R_{-1},t)+\frac{h_{-1}}{h_{-2}(h_{-1}+h_{-2})}\psi^{i}_{Bn}(R_{-2},t)=0, \tag{27}$$

where R_1 and R_2 are R-values at the first and second grid point from $R=1$ outward, respectively, $h_0=R_1-1$, and $h_1=R_2-R_1$. Eq. (25) leads to

$$\psi_{Bn}(R_\infty,t)=0 \quad (n\geqslant 1). \tag{28}$$

2.6. Auxiliary conditions

Since the point $R=0$ is by no means a singular point, as a necessary condition the following hold:

$$\psi_n(0,t)=\zeta_n(0,t)=\psi_{Bn}(0,t)=\zeta_{Bn}(0,t)=0 \quad (n\geqslant 1). \tag{29}$$

2.7. A non-uniform grid spacing in R (the internal region of a liquid meal)

To support high Reynolds and Strouhal number cases, introduced is a non-uniform grid spacing in R, where the nth coordinate R_{-n} numbered from the free surface is specified, using a suitable positive constant γ (h: a constant to be determined to satisfy such a condition that $R=0$ is on a grid), by

$$R_{-n}=R_0-h\left(\frac{\sinh(n-1)\gamma}{\sinh\gamma}+1\right). \tag{30}$$

An uniform grid spacing in R is made as γ approaches +0, and the larger γ produce the denser grid spacing near R_0.

2.8. Numerical integration schemes

The Fourier series (18) can be truncated up to a suitable order and governing equations can be split into corresponding Fourier components to constitute a simultaneous partial differential equations in R and t, which can be integrated semi-implicitly with respect to time by starting from at rest with a no magnetic field [$\psi(R,\beta,0)=\zeta(R,\beta,0)=\zeta_B(R,\beta,0)=0$ $(0\leqslant R<1)$, $\psi_B(R,\beta,0)=0$ $(0\leqslant R<R_\infty)$] to get a periodic solution in time.

2.9. Dimensionless force and levitation radius

From Eqs. (3), (19) and (20), dimensionless levitation force L_z is given by

$$L_z(t)=\pi\int_0^\pi\left\{\left(B_\alpha^2-B_\beta^2\right)r\frac{\partial r}{\partial\beta}\right\}_{R=1}\mathrm{d}\beta-\frac{4\pi}{Re}\int_0^\pi\left\{\frac{1}{\sqrt{J}}\frac{\partial(rv_\beta)}{\partial\beta}\frac{\partial r}{\partial\beta}\right\}_{R=1}\mathrm{d}\beta+\pi\int_0^\pi\left(\frac{\partial P^*}{\partial\beta}r^2\right)_{R=1}\mathrm{d}\beta, \tag{31}$$

$$\frac{\partial P^*}{\partial\beta}=\frac{1}{Re}\frac{R}{r}\frac{\partial(r\zeta)}{\partial R}+\sqrt{J}\zeta_B B_\alpha-\left(\sqrt{J}\frac{\partial v_\beta}{\partial t}+v_\beta\frac{\partial v_\beta}{\partial\beta}\right), \tag{32}$$

where v_β is the dimensionless velocity component in the β-direction and P^* is the dimensionless pressure based on B_0^2/μ_m. The dimensionless magnetic force component in the z-direction is defined as

$$\begin{aligned} M_z(t) &\equiv \pi \int_0^\pi \left\{ \left(B_\alpha^2 - B_\beta^2 \right) r \frac{\partial r}{\partial \beta} \right\}_{R=1} \mathrm{d}\beta + 2\pi \int_0^\pi \left(B_\alpha B_\beta r \frac{\partial z}{\partial \beta} \right)_{R=1} \mathrm{d}\beta \\ &= \frac{1}{a^2 B_0^2/\mu_m} \int\int\int (\boldsymbol{j} \times \boldsymbol{B})_z \, \mathrm{d}V, \end{aligned} \tag{33}$$

where $\mathrm{d}V$ is the volume element of a liquid metal. Time mean values of dimensionless levitation and magnetic force, L_m and M_m, are given by

$$L_m \equiv \frac{1}{T_m} \int_t^{t+T_m} L_z \, \mathrm{d}t, \quad M_m \equiv \frac{1}{T_m} \int_t^{t+T_m} M_z \, \mathrm{d}t, \tag{34}$$

respectively, where T_m is the period in time. The dimensionless levitation radius of a sphere (the gravity force acting to which is equal to levitation force) based on $\sqrt[3]{\mu^2/(\rho^2 g)}$ is

$$K = \sqrt[3]{\frac{3}{4\pi} Re^2 L_m}. \tag{35}$$

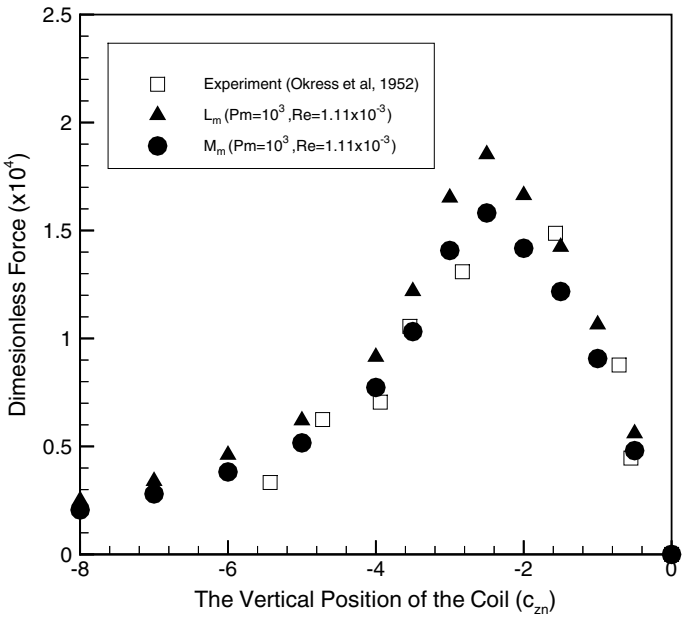

Fig. 2. Comparison of dimensionless force between computed data and experimental data at $Re \cdot P_m = 1.11$, $St = 183$ and the dimensionless horizontal coil position $c_{rn} = 4.85$.

3. Numerical results

(i) Common conditions under numerical computation.
All the numerical computation is executed at a time interval of $2\pi/(St \cdot 100)$ with $A_{\text{coil}}/a^2 = \pi/16$, $h_n = \sqrt{\pi}/4$ and $I_{kn} = 1$.

(ii) Force against a vertical coil position.
Dimensionless force (L_m and M_m) corresponding to a highly viscous state is plotted in Fig. 2 against a dimensionless vertical coil position c_{zn} in case of a single-loop coil with the experimental data ($Re \cdot P_m = 1.11$, $St = 183$, the dimensionless horizontal coil position $c_{rn} = 4.85$) by Okress et al [3], which shows qualitatively good agreement of computed data with experimental ones for a solid metal. While difference between L_m and M_m, i.e., contribution from pressure and viscous terms is small.

(iii) Force against a Strouhal number.
Magnitude of dimensionless force, $|L_m|$ and $|M_m|$, is plotted in Fig. 3 against a Strouhal number St at $Re = 10^{-3}$, $(c_{zn},c_{rn}) = (-1.4,1.4)$, $P_m = 10^3$ (ideally high viscosity) or $P_m = 9.7 \times 10^{-7}$ (Fe at a melting point). The sign change of L_m at $P_m = 9.7 \times 10^{-7}$ will take place at higher St than that at $P_m = 10^3$.

(iv) $B_\alpha(1,\beta,t)$, $B_\beta(1,\beta,t)$ and $v_\beta(1,\beta,t)$.
Free surface magnetic flux density components $B_\alpha(1,\beta,t)$, $B_\beta(1,\beta,t)$ and a surface velocity component $v_\beta(1,\beta,t)$ are plotted in Figs. 4(a)–(c), respectively, at $Re = 10^{-3}$, $(c_{zn},c_{rn}) = (-1.4,1.4)$, $P_m = 10^3$ and time t when ζ_B reaches maximum, and those in Figs. 4(d)–(f), respectively, at the same condition except $P_m = 9.7 \times 10^{-7}$.

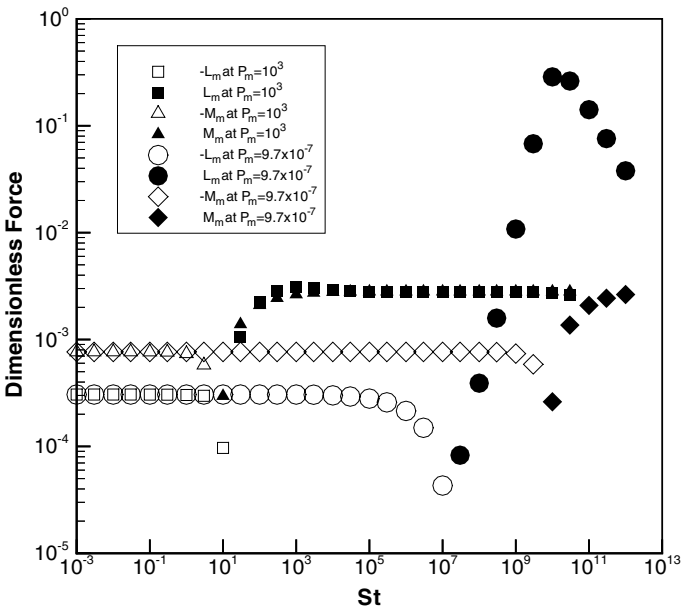

Fig. 3. Comparison of dimensionless force between $P_m = 10^3$ and $P_m = 9.7 \times 10^{-7}$ at $Re = 10^{-3}$ and the coil position $(c_{zn},c_{rn}) = (-1.4,1.4)$.

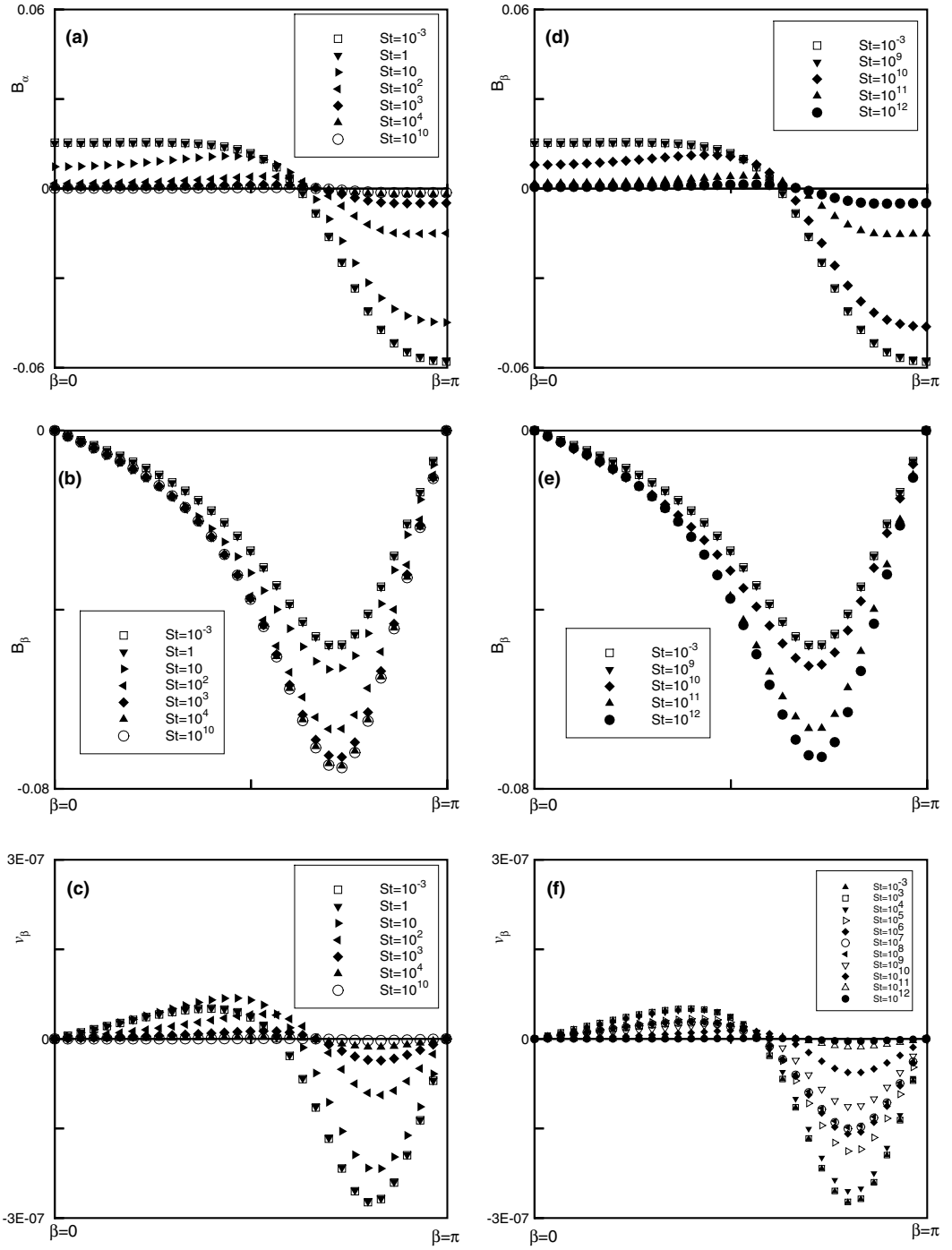

Fig. 4. Graphs of $B_\alpha(1,\beta,t)$, $B_\beta(1,\beta,t)$ and $v_\beta(1,\beta,t)$ at $Re = 10^{-3}$, the coil position $(c_{zn},c_{rn}) = (-1.4,1.4)$ and time t when ζ_B reaches maximum: (a)–(c) $P_m = 10^3$; (d)–(f) $P_m = 9.7 \times 10^{-7}$.

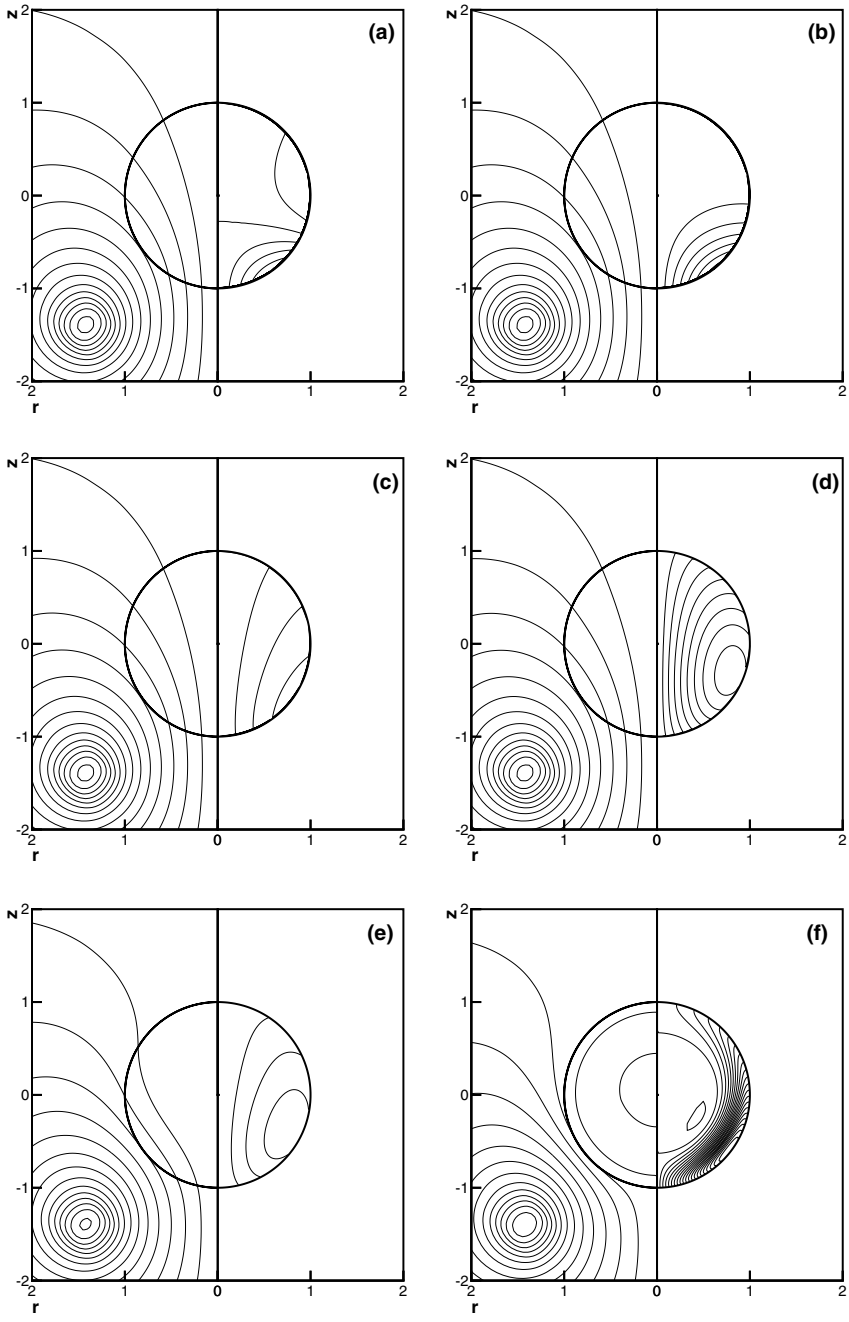

Fig. 5. Magnetic field solutions at $P_m = 9.7 \times 10^{-7}$, $Re = 10^{-3}$, the coil position $(c_{zn},c_{rn}) = (-1.4,1.4)$ and time t when ζ_B reaches maximum; contour lines of ψ_B ($\delta\psi_B = 5 \times 10^{-3}$); contour lines of the dimensionless magnetic vorticity on right. (a) $St = 10^5$, $\delta\zeta_B = 2 \times 10^{-6}$; (b) $St = 10^7$, $\delta\zeta_B = 2 \times 10^{-6}$; (c) $St = 10^8$, $\delta\zeta_B = 2 \times 10^{-5}$; (d) $St = 10^9$, $\delta\zeta_B = 2 \times 10^{-4}$; (e) $St = 10^{10}$, $\delta\zeta_B = 0.02$; (f) $St = 10^{11}$, $\delta\zeta_B = 0.02$.

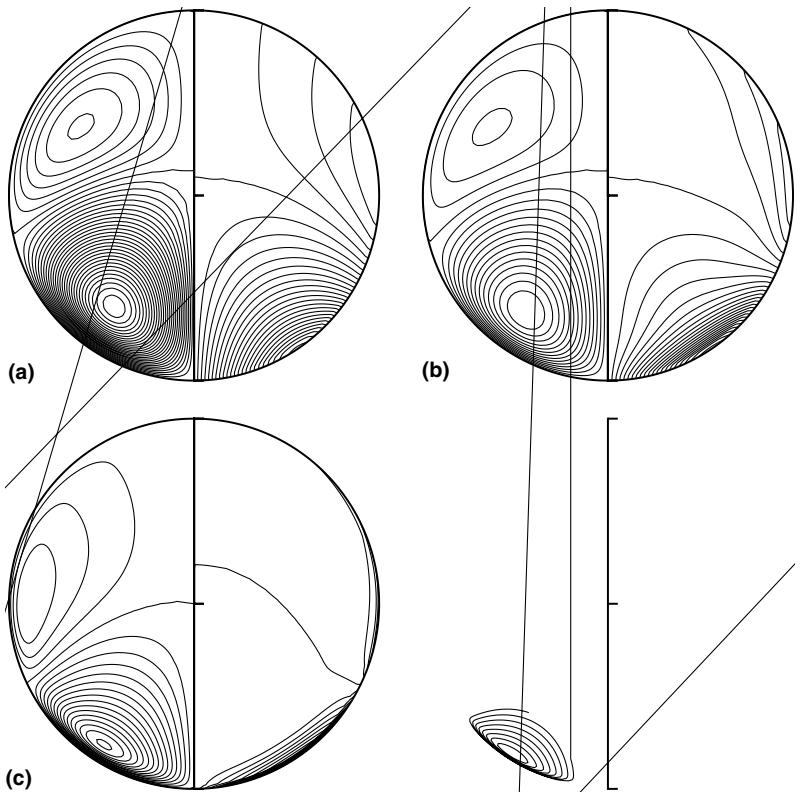

(v) Contour lines of ψ_B and ζ_B with St at a single coil.
Contour lines of ψ_B and ζ_B for a single coil are shown in Figs. 5(a)–(f) for various St at $P_m = 9.7 \times 10^{-7}$(molten Fe), $Re = 10^{-3}$, $(c_{zn},c_{rn}) = (-1.4,1.4)$ and time t when ζ_B reaches maximum. At the highest Strouhal number St of 10^{11}, magnetic vorticity is found to be concentrated to the surface of a liquid metal.

(vi) Contour lines of ψ and ζ with St at a single coil.
Contour lines of ψ and ζ are shown in Figs. 6(a)–(d) for various St at $P_m = 9.7 \times 10^{-7}$(molten Fe), $Re = 10^{-3}$, $(c_{zn},c_{rn}) = (-1.4,1.4)$ and time t when ζ_B reaches maximum.

(vii) Variation of $|L_m|$ with St and Re at a single coil.
Variation of $|L_m|$ with St and Re is shown in Figs. 7(a) and (b), respectively, at $P_m = 9.7 \times 10^{-7}$ and $(c_{zn},c_{rn}) = (-1.4,1.4)$.

(viii) Contour lines of ψ_B, ζ_B, ψ and ζ with Re at a single coil.
Contour lines of ψ_B and ζ_B at $Re = 10^2$ and 10^4 are shown in Figs. 8(a) and (e), respectively, and those of ψ and ζ at $Re = 10^2$, 10^3, 3×10^3 and 10^4 are shown in Figs. 8(b), (c), (d), (f), respectively. The absolute value of ψ at the bottom circularity center increases with Re as found in Figs. 8(b), (c), (d), (f).

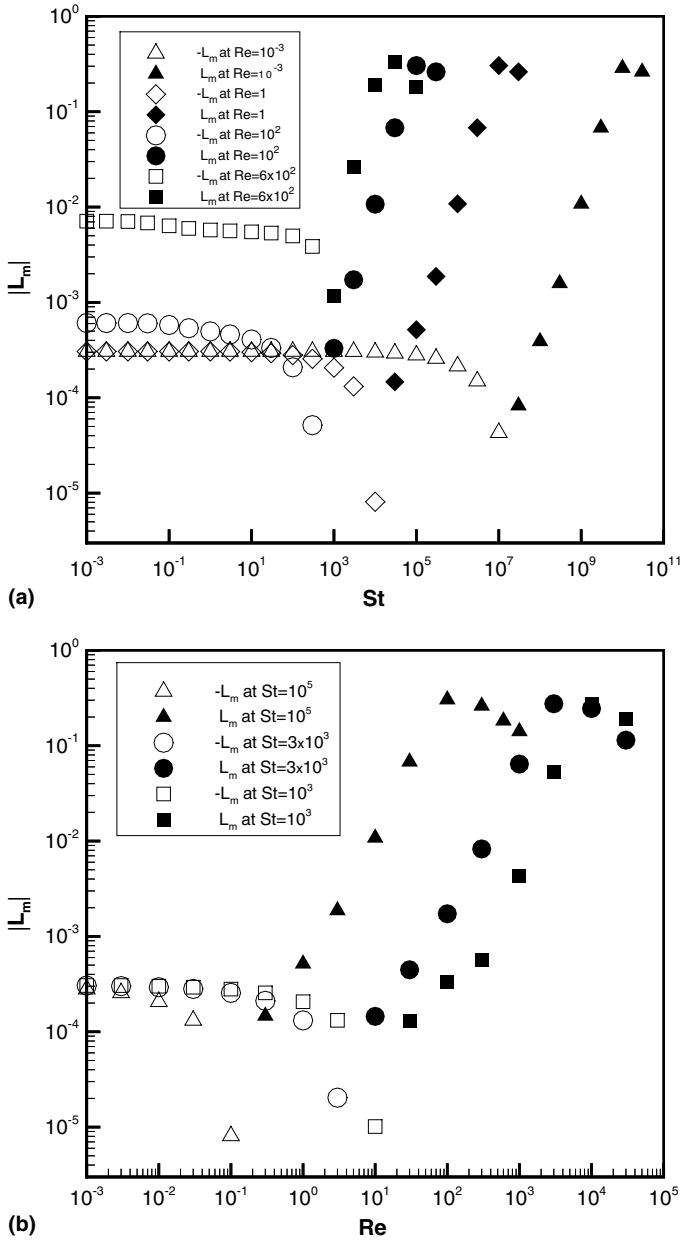

Fig. 7. Variation of $|L_m|$ at $P_m = 9.7 \times 10^{-7}$ and the coil position $(c_{zn},c_{rn}) = (-1.4,1.4)$.

(ix) Variation of $|L_m|$ and K for various coil configurations.
Variation of $|L_m|$ for various coil configurations at $Re = 10$ with St and that at $St = 10^4$ with Re are shown in Figs. 9(a) and (b), respectively, while variation of K at $Re = 10$ with St and that at $St = 10^4$ with Re are shown in Figs. 9(c) and (d), respectively.

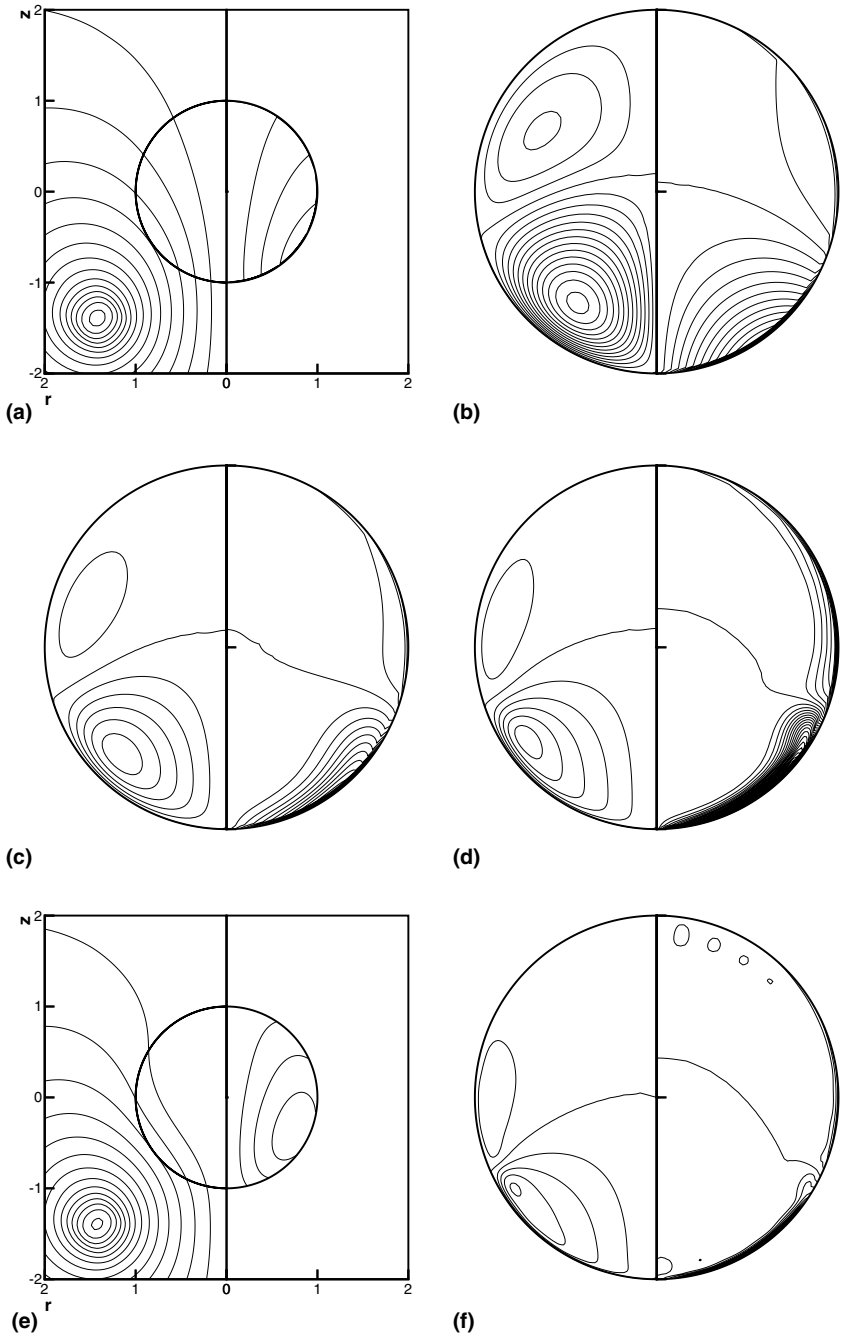

Fig. 8. Solutions of both the magnetic field and the flow field at $St = 10^3$, $P_m = 9.7 \times 10^{-7}$, the coil position $(c_{zn}, c_{rn}) = (-1.4, 1.4)$ and time t when ζ_B reaches maximum. (a) $Re = 10^2$, $\delta\psi_B = 5 \times 10^{-3}$, $\delta\zeta_B = 2 \times 10^{-5}$; (b) $Re = 10^2$, $\delta\psi = 10^{-4}$, $\delta\zeta = 0.01$; (c) $Re = 10^3$, $\delta\psi = 10^{-3}$, $\delta\zeta = 0.1$; (d) $Re = 3 \times 10^3$; $\delta\psi = 10^{-3}$, $\delta\zeta = 0.1$; (e) $Re = 10^4$, $\delta\psi_B = 5 \times 10^{-3}$, $\delta\zeta_B = 0.02$; (f) $Re = 10^4$, $\delta\psi = 10^{-3}$, $\delta\zeta = 1$.

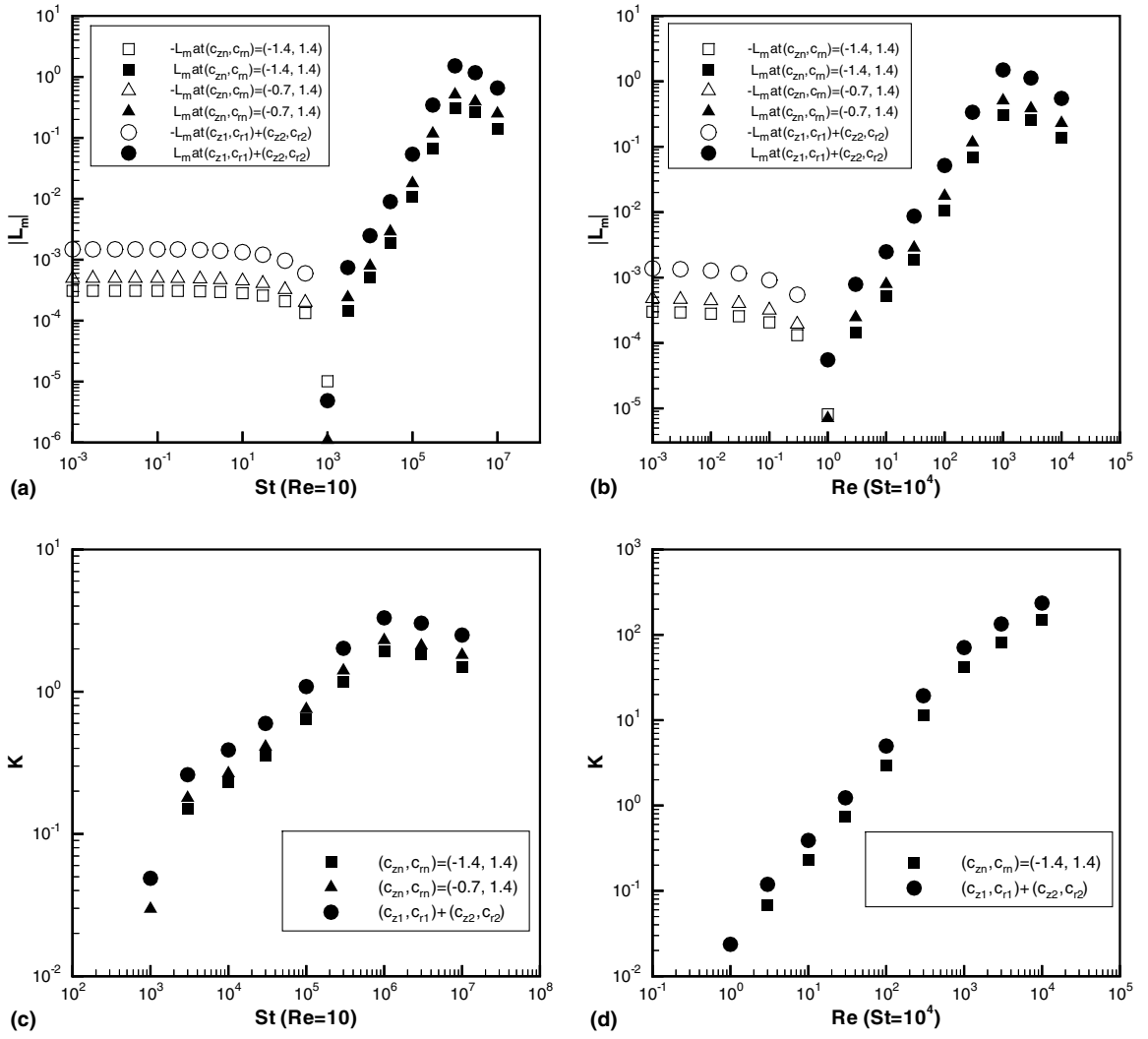

Fig. 9. Comparison of $|L_m|$ (a, b) and K (c, d) among $(c_{zn},c_{rn}) = (-1.4,1.4)$, $(c_{zn},c_{rn}) = (-0.7,1.4)$ and $(c_{z1},c_{r1}) + (c_{z2},c_{r2})$ at $P_m = 9.7 \times 10^{-7}$, where $(c_{z1},c_{r1}) = (-1.4,1.4)$ and $(c_{z2},c_{r2}) = (-0.7,1.4)$.

(x) Contour lines of ψ_B, ζ_B, ψ and ζ with Re at two external coils.
Contour lines of ψ_B and ζ_B for two external coils are shown in Figs. 10(a)–(f) for various Re at $P_m = 9.7 \times 10^{-7}$, $St = 10^4$, two coils and time t when ζ_B reaches maximum, whereas those of ψ and ζ for two external coils are shown in Figs. 11(a)–(f) for various Re at $P_m = 9.7 \times 10^{-7}$, $St = 10^4$, two coils and time t when ζ_B reaches maximum.

(xi) The magnetic Prandtl number of a liquid metal.
Although numerical calculation for the liquid metal is performed at $P_m = 9.7 \times 10^{-7}$ (Fe at the melting point), numerical results are not limited qualitatively to iron because liquid metals have low magnetic Prandtl numbers (about $10^{-7} \sim 10^{-5}$). Table 1 shows that a difference between levitation forces L_m at $P_m = 9.7 \times 10^{-7}$ and $P_m = 2.6 \times 10^{-6}$ (Al at the melting point) is small.

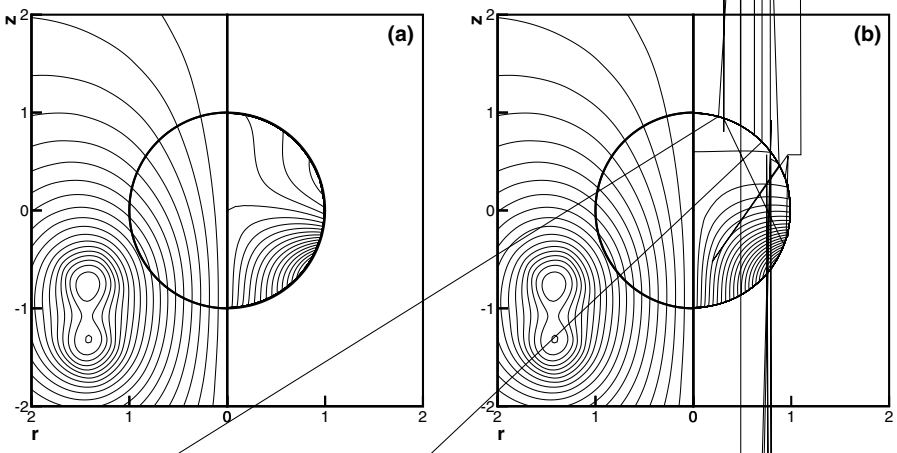

(e)

0

1

Table 1
Values of L_m at $St = 10^4$

P_m	Re				
	10^{-2}	10^{-1}	1	10	10^2
9.7×10^{-7}	-2.8×10^{-4}	-2.1×10^{-4}	-8.1×10^{-6}	5.2×10^{-4}	1.1×10^{-2}
2.6×10^{-6}	-2.8×10^{-4}	-2.1×10^{-4}	-6.6×10^{-6}	6.4×10^{-4}	2.1×10^{-2}

4. Conclusions

It is demonstrated that, with proper transformation of governing equations and boundary conditions, it is possible to obtain unsteady-state periodic solutions of liquid metals in a vertical axisymmetric levitation melting, using a spectral finite difference method. Levitation force, magnetic force, magnetic fields and flow fields were presented for several parameters. Numerical data for high viscosity on dimensionless force with the dimensionless vertical coil position are qualitatively in good agreement qualitatively with experimental data for a solid metal [3]. The effects of the Reynolds number, the Strouhal number and the number of the external coil(s) on levitation force, the magnetic field and the flow field are clarified, with a peak of levitation force against a Strouhal number at a constant Reynolds number or Reynolds number at a constant Strouhal number.

References

[1] I. Egry, G. Lohoefer, G. Jacobs, Surface tension of liquid metals: results from measurements on ground and in space, Phys. Rev. Lett. 75 (1995) 4043–4046.
[2] I. Egry, A. Diefenbach, W. Dreier, J. Piller, Containerless processing in space – thermophysical property measurements using electromagnetic levitation, Int. J. Thermophys. 22 (2001) 569–578.
[3] E.C. Okress, D.M. Wroughtom, G. Comenetz, P.H. Brace, J.C.R. Kelly, Electromagnetic levitation of solid and molten metals, J. Appl. Phys. 23 (1952) 545–552.
[4] A.J. Mestel, Magnetic levitation of liquid metals, J. Fluid Mech. 117 (1982) 27–43.
[5] A. Gagnoud, J. Etay, M. Garnier, The levitation melting process using cold crucible technique, Trans. ISIJ 28 (1988) 36–40.
[6] H. Tadano, M. Fujita, T. Take, K. Nagamatsu, A. Fukuzawa, Levitational melting of several kilograms of metal with a cold crucible, IEEE Trans. Magn. 30 (1994) 4740–4742.
[7] S. Berry, R.W. Hyers, B. Abedian, L.M. Racz, Modeling of turbulent flow in electromagnetically levitated metal droplets, Metall. Mater. Trans. B 31 (2000) 171–178.
[8] V. Shatrov, V. Galindo, G. Gerbeth, Stablity analysis of the flow inside an electromagnetically levitated drop, Magneohydrodynamics 37 (2001) 45–54.
[9] V. Bojarevics, K. Pericleous, Magnetic levitation fluid dynamics, Magneohydrodynamics 37 (2001) 93–102.
[10] Y. Mochimaru, Effectiveness of a spectral finite difference scheme, Comput. Fluid Dyn. Rev. 1 (1998) 379–394.
[11] Y. Mochimaru, Numerical simulation of flow past a circular cylinder under a magnetic field, Comput. Fluids 21 (1992) 177–184.
[12] K. Im, Y. Mochimaru, Numerical analysis on a flow field of liquid metals under a magnetic field using a spectral finite difference scheme, JSME Int. J. Ser. B 46 (2003) 349–355.